HIAPER Pole-to-Pole Observations (HIPPO): fine-grained, global-scale measurements of climatically important atmospheric gases and aerosols

HIAPER Pole-to-Pole Observations (HIPPO): Fine grained, global scale measurements of climatically important atmospheric gases and aerosols

S. Wofsy, the HIPPO Science Team, and cooperating modelers and satellite teams:

Harvard University, Cambridge, MA, USA:
S. C. Wofsy, B. C. Daube, R. Jimenez, E. Kort, J. V. Pittman, S. Park, R. Commane, Bin Xiang, G. Santoni, D. Jacob, J. Fisher, C. Pickett-Heaps, H. Wang, K. Wecht, Q.-Q. Wang;

National Center for Atmospheric Research, Boulder, CO USA:
B. B. Stephens, S. Shertz, P. Romashkin, T. Campos, J. Haggerty, W. A. Cooper, D. Rogers, S. Beaton, R. Hendershot;

NOAA ESRL and CIRES, Boulder, CO USA:
J. W. Elkins, D. W. Fahey, R. S. Gao, F. Moore, S. A. Montzka, J. P. Schwarz, D. Hurst, B. Miller, C. Sweeney, S. Oltmans, D. Nance, E. Hintsa, G. Dutton, L. A. Watts, J. R. Spackman, K. H. Rosenlof, E. A. Ray, B. Hall;

Princeton University, Princeton, NJ USA: M. A. Zondlo, M. Diao

University of California at San Diego: R. Keeling, J. Bent;

University of Miami, Miami, FL: E. L. Atlas, R. Lueb

Jet Propulsion Laboratory, Pasadena, CA: M. J. Mahoney, M. Chahine, E. Olsen;

Research Institute for Global Change, JAMSTEC: P. Patra, K. Ishijima

European Centre for Medium-Range Weather Forecasts, Reading, United Kingdom:
R. Engelen, J. Flemming;

University of Toronto, Toronto, Canada: R. Nassar, D. B. A. Jones;

National Institute for Water and Atmospheric Research, Wellington, New Zealand: S. E. Mikaloff Fletcher

Abstract

The HIAPER Pole-to-Pole Observations (HIPPO) program has completed three of five planned aircraft transects spanning the Pacific from 85N to 67S, with vertical profiles every ~2.2° of latitude. Measurements include greenhouse gases, long-lived tracers, reactive species, O_2/N_2 ratio, black carbon, aerosols, and CO_2 isotopes. Our goals are to address the problem of determining surface emissions, transport strength and patterns, and removal rates of atmospheric trace gases and aerosols at global scales, and to provide strong tests of satellite data and global models. HIPPO data show dense pollution and black carbon at high altitudes over the Arctic, imprints of large N_2O sources from tropical lands and convective storms, sources of pollution and biogenic CH_4 in the Arctic, and summertime uptake of CO_2 and sources for O_2 at high southern latitudes. Global chemical signatures of atmospheric transport are imaged, showing remarkably sharp horizontal gradients at airmass boundaries, weak vertical gradients, and inverted profiles (maxima aloft) in both hemispheres. These features challenge satellite algorithms, global models, and inversion analyses to derive surface fluxes. HIPPO data can play a crucial role in identifying and resolving questions of global sources, sinks and transport of atmospheric gases and aerosols.

Introduction

Future action on climate change requires us to be able to distinguish surface emissions of greenhouse gases directly associated with human activities from indirect effects of climate change and from natural variations. Measurements of concentrations of greenhouse gases ("GHGs") such as CO_2, CH_4, and N_2O, and tracers (e.g. CO, SF_6, O_2/N_2) have been used to derive surface fluxes, and to attribute emissions to human activity or natural processes, in a variety of conceptual frameworks (Bey et al., 2001; Gurney et al., 2002; Engelen et al., 2009; Kort et al., 2008; Michalak et al., 2004; Patra et al., 2009). A common approach is to exercise atmospheric chemistry-transport models (ACTMs) to simulate concentrations of pollutants in time and space over the globe, typically combining *a priori* surface emission flux fields, rates for chemical reactions in the atmosphere, and assimilated meteorological fields. The surface flux field is then adjusted to obtain the best match between model output and data. The model is effectively "inverted" to define optimal sources and sinks from atmospheric concentrations.

Global scale ACTMs have difficulty resolving sharp chemical gradients, such as exist at airmass boundaries, at the tropopause (Pan et al., 2010; Ishijima et al., 2010) or in plumes of tracers emanating from strong source regions, a limitation inherent in the numerical methods used in the Eulerian model framework [Rastigejev et al., 2010]. ACTM outputs are commonly compared to data sets that likewise do not resolve sharp gradients or define fine scale variance and covariance, e.g. data from sparse ground stations or satellites. These data are in some respects ideal for comparison with global simulations, since they may be presumed to represent large air masses and global-scale processes. But because accurate knowledge of vertical and horizontal gradients is available neither from global data nor from global models, the fine-grained structure of atmospheric tracer distributions is unknown and we have no way to assess how important this structure might be for inverse models.

Air mass boundaries move in space and time. Spatially aggregated data, or measurements from widely spaced locations (e.g. remote island stations), give horizontal patterns with diffuse boundaries. This fuzzy picture might be correct if data are averaged over time (e.g. for a month), but the pattern is never actually present in the atmosphere. A model may reproduce these smoothed gradients with simulated rates of transport across air mass boundaries that are significantly in error, leading to incorrect surface fluxes inferred from an inverse analysis. Similarly, if the vertical gradient in a model is systematically in error, the atmospheric mass burden (or column integral) is improperly simulated and significant bias can result when the model is inverted to obtain optimal surface fluxes [e.g. Stephens et al., 2007].

Surface fluxes obtained by inverting global models are also subject to systematic errors derived from other elements of the model framework, in addition to transport errors. For example, misidentification of source processes and locations, or incorrectly specified temporal variation of *a priori* fluxes, introduce errors into "optimal" flux fields associated directly with model constructs. Since generally the only adjustable parameters in an inverse model are surface fluxes, strong, independent tests of all elements of the model framework are needed, using atmospheric measurements, in order to reduce the impact of these diverse systematic errors and biases.

This paper introduces the data obtained by the HIAPER Pole-to-Pole Observations ("HIPPO") project, a sequence of five global aircraft measurement programs that sample the atmosphere from (almost) the North Pole to the coastal waters of Antarctica, from the surface to 14 km, spanning the seasons. Three have been completed to date—January and November, 2009, April, 2010, to be followed by June and August/September, 2011 (denoted HIPPO-1, 2, etc). This paper will focus primarily on results obtained in HIPPO-1, for which data have been finalized.

HIPPO is intended to obtain global scale, fine-grained data for the first time, for a large number of atmospheric constituents. HIPPO data provide high resolution, systematic, pole-to-pole curtains with deeper vertical extent than possible in the past, acquired at high temporal resolution to preserve correlations among constituents. The goal is to provide new perspectives on how to use data to wring out transport issues in ACTMs, to identify and address the errors in the spatial/temporal representation of surface fluxes and reaction rates, to discover new features of trace gas and aerosol emissions and global-scale transport, and to rigorously test satellite algorithms. A related goal is to elucidate the underlying processes and controls on surface emission fluxes, in order to be able to predict emissions and atmospheric concentrations in the future.

Fine-grained data have been obtained previously from aircraft platforms, but only a few data sets have long transects covering extended time periods, principally from commercial airliners that acquire data exclusively at cruise altitude plus vertical profiles entering/leaving large urban complexes [Nakazawa et al., 1991; Machida et al., 2008; Marenco et al., 1998]. High-resolution data sets spanning the depth of the atmosphere over large areas are available from a few surveys [Davis, 1980; Hoell et al., 1999; Jacob et al., 2003; Raper et al., 2001] that covered much smaller domains and seasonal intervals than HIPPO. Thus HIPPO data provide hitherto unavailable information for testing and refining understanding of global distributions and surface fluxes of trace gases and aerosols.

HIPPO payload

HIPPO measurements are summarized in Table 1. The platform is the National Science Foundation's Gulfstream V ("GV" or "HIAPER") aircraft operated by the

National Center for Atmospheric Research (NCAR). Major greenhouse gases (CO_2, CH_4, N_2O) and other important trace species (CO, SF_6, O_2/N_2, H_2, etc) were measured at high frequency, many at 1 Hz, with two (or more) independent measurements for each to provide redundancy (5 for CO_2), check calibration and assess sensor drift. The Quantum Cascade Laser Spectrometer (QCLS), which measures CO_2, CO, CH_4, and N_2O, is a mid-infrared sensor developed by Harvard University and Aerodyne Corp., owned by NCAR, and operated during HIPPO by the Harvard team; "OMS" is a Harvard CO_2 sensor using an infrared gas analyzer (IRGA), which has logged > 300 flights on airborne platforms (Daube et al., 2002). RAF-CO refers to NCAR's AeroLaser AL5002 vacuum-UV sensor. Data at 1 Hz were obtained in two independent measurements for O_3 and for H_2O (by VCSEL, a new open path near-IR multi-pass spectrometer (Zondlo et al., 2010), and UCATS-H_2O, a NOAA mid-IR spectrometer with a sampling inlet). AO2 is the NCAR Airborne Oxygen Instrument, which measures O_2 using a vacuum-ultraviolet absorption technique (Stephens et al., 2003) and CO_2 using a single-cell IRGA (Licor 850). UCATS and PANTHER are on-board gas chromatographs with extensive flight histories, measuring at 1-3 minute intervals.

A comprehensive suite of greenhouse gases and a diverse ensemble of halocarbons, hydrocarbons, and sulfur species were measured by the Whole-Air Sampler system ("WAS", Pan et al., 2010), utilizing three different collection systems: stainless steel electropolished cylinders ("AWAS" from University of Miami), glass vessels from the NOAA "PFP" program ("NWAS" from NOAA) and special glass vessels for measuring O_2/N_2 and Ar/N_2 ratios, and the isotopic composition of CO_2 ("MEDUSA" from University of California at San Diego).

Black carbon (BC) was measured at 1 Hz by the NOAA Single-Particle Soot Photometer (SP2) [Schwarz et al., 2008] on air drawn into the cabin. The SP2 uses a laser beam to heat the BC component of individual fine-mode aerosol particles to vaporization, resulting in emission of thermal radiation that is interpreted to give the BC mass concentration and size distribution. Other particle probes, including a Cloud Droplet Probe (CDP), the NCAR UHSAS aerosol sensor, the 2D-C Particle Imager, and the PMS Liquid Water Sensor (King) (PLWC), resided on the wing, along with the Microwave Temperature Profiler ("MTP"), which measures the temperature profile above and below the plane, and a digital camera that acquired an image every second.

Results

Figure 1 shows the flight tracks for HIPPO-1 and -2, plus vertical sampling and observed isentropic structure for HIPPO-1. Each deployment obtained a southbound cross section of the atmosphere near the International Dateline, covering the Arctic Ocean, Alaska, and the entire Pacific to just short of Antarctica. Northbound, HIPPO-1 traversed the South Pacific to sample in the Eastern Tropical Pacific upwelling zone, and HIPPO-2 sampled the Western Pacific warm pool. We obtained 138, 151, and 136 vertical profiles in HIPPO-1, -2, and -3 respectively, spanning 67^{o}S to 80^{o}N.

On average consecutive samples in the mid-troposphere are separated by 2.2° of latitude, with 4.4° between consecutive near-surface or high altitude samples. Most profiles extended from ~300m to 8500m altitude, constrained by air traffic, but significant profiling extended above ~14 km (Fig. 1c).

Figure 1d shows the cross section of potential temperature (Θ) versus latitude and GPS altitude (MASL) during HIPPO-1. A dome of very cold, stable air, with a strong latitude gradient of Θ, covered the Arctic, with a sharp transition at the northern edge of the polar jet, near 60°N. There was a narrow zone of stratospheric influx just equatorward of 60 N, and then a belt of much weaker vertical stratification from 60 to 40N, the region of the "warm conveyor belt" where vertical transport occurs in association with jet stream dynamics and midlatitude storms [Bethan et al., 1998; Cooper et al., 2004]. Equatorward of 40°N there was a broad Θ bulge in the middle and upper troposphere, reflecting the influence of deep convection and the Hadley circulation. The southern hemisphere had similar structure, but the features were weaker, reflecting the summer season.

Figure 2 shows cross sections along the dateline for key species in January 2009 (HIPPO-1). Atmospheric tracers displayed sharp transitions in the horizontal, demarcating the boundaries between polar, middle latitude, subtropical, and tropical air masses, and at the Intertropical Convergence Zone ("ITCZ", the persistent line of convective storms that circles the globe near the equator, demarcating the boundary between the hemispheres). Gradients were much weaker in the vertical than in the horizontal, except in the northern polar region where fresh inputs of CO, CO_2, CH_4, and SF_6 were evidenced by high values near the surface and the presence of very short-lived pollutants (e.g. benzene). According to model simulations (discussed further below), these pollutants originated from Asia and Europe. In the Arctic, tracer isopleths broadly aligned with isentropes, with sporadic anomalies due to proximate emissions or with stratospheric influence. Convective transport across isentropes was evident elsewhere, in midlatitudes, tropics, and subtropics, particularly for the longest-lived tracers (e.g. SF_6 and N_2O). The peak value of SF_6 over the North Pacific was observed in the middle troposphere. Concentrations of N_2O showed a completely different pattern compared to other greenhouse gases, with a prominent bulge in the middle and upper tropical and subtropical troposphere, plus sporadic enhancements between 10 and 14 km. Similar features were seen for N_2O in all three missions flown so far.

Water vapor showed the expected increases with temperature and tropical origin. Input of very wet air was notable in the South Pacific Convergence Zone ("SPCZ", 10-20 S). The SPCZ is a persistent frontal formation of widespread cloud cover and precipitation extending in a southeast direction from New Guinea into the Southern Hemisphere (SH) midlatitudes, with strong convection typically extending over a large area. It id specially prominent in boreal winter [Widlansky, 2007]. The SPCZ is spatially larger, and contains more intense convection, than similar convergence zones elsewhere, such as the South Indian Convergence Zone (SICZ) and the South

Atlantic Convergence Zone (SACZ), although it is not clear why [Widlansky, 2007]. Analogous, but less distinct, anomalies have been observed for other chemical tracers near the SPCZ (Gregory et al., 1999; Mari et al., 2003). In each of the three HIPPO missions so far, the water vapor plume from the SPCZ has been larger in extent, and penetrated deeper into the atmosphere, than in the ITCZ. These results suggest that the SPCZ may be an important global source of water vapor to the tropical tropopause layer over the Pacific, at least in the boreal winter season, supporting inferences from observations of cirrus clouds over the tropical western Pacific during that season (Fujiwara et al., 2009).

Figure 3 shows cross sections for HIPPO-2 in November 2009. Inverted vertical profiles (i.e., with higher concentrations aloft) were surprisingly strong. Pollutant levels typical of urban corridors were found in a thick layer at 6-8 km over an extensive region of the Arctic, overlying clean air. The layers preserve coherence (*panels d, e*) among tracers despite sharp gradients and transport over thousands of kilometers, with strong vertical uplift. Very high levels of black carbon aerosol were present, and absorption of solar radiation was visible (*panel c*). High aerosol concentrations indicate the absence of efficient precipitation scavenging, suggesting that polluted air was lofted by isentropic advection over the cold dome that was in the process of developing over the Arctic. Notable enhancements of N_2O were observed in some of the plumes. In many descents, enhanced CH_4 concentrations were observed near the surface of the Arctic Ocean, sometimes in otherwise pristine air, possibly signifying emission from biogenic sources or from CH_4 hydrates (e.g. Fig. 3c, below 2000m). Horizontal gradients were again very sharp at air mass boundaries.

Figure 4 illustrates the meridional gradients of CO_2 and O_2/N_2. Concentrations of CO_2 were enhanced *above* the surface (but not *at* the surface) from 45 S to 70 S in January (Figs. 2c, 4a), which might confirm a signal of elevated CO_2 in this region similar to that reported by the AIRS satellite[Chahine et al., 2008]; the structure of the CO_2 distribution is rather complex, with likely contributions from multiple processes including fires in Australia and uptake of CO_2 at the ocean surface. There is excess O_2 near the surface all the way from 20S to 60S (Fig. 4b), reflecting inputs to the atmosphere from both the ocean and the land, including thermal degassing of O_2 from the ocean and biological production of O_2 from land and ocean in summer.

Preliminary simulations of HIPPO-1 data have been made with global models including GEOS-CHEM [Bey et al., 2001], ACTM [Patra et al., 2009], and GEMS/MACC [Hollingsworth et al., 2009]. Examples are shown in Figs. 4c and 5a-d. The models extracted computed values along the flight track for detailed comparison to HIPPO. Model simulations performed reasonably well in many respects, as can be seen by comparing with Figure 2. Simulations of CO_2 from the GEOS-CHEM model (Nassar et al., 2010; Fig. 5a) captured many features of the observations (Fig. 2c), including the relatively well-mixed profiles in subpolar and middle latitudes. Vertical contrasts occurred mostly over the Arctic and Antarctic/Southern Ocean, reflecting inputs from fossil fuels and marine biological uptake, respectively. But horizontal

gradients were much sharper in the atmosphere, and vertical gradients weaker, than in the models. Most satellite data likewise do not resolve the observed gradients. Enhanced CO_2 poleward of 40°S seen by HIPPO is not reproduced in the model (compare Fig. 4a and 2c); the major pollution signature appears at 60°N instead of 80°N; enhanced surface CO_2 in the southern hemisphere deep tropics, likely from equatorial upwelling, is not simulated in the model.

Both the ACTM and GEOS-Chem models appear to have vertical transport rates that are too weak at high latitudes (compare CO_2, SF_6 and CO in Fig. 5 to Fig.2), both along and across isentropes. The MACC-GEMS model gives a somewhat better appearance for vertical profiles of CO and CH_4 (not shown), but has anomalies elsewhere and misses global scale North-South gradients significantly: MACC-GEMS predicts 70 ppb for ΔCO between the Antarctic and the Arctic, compared to ~95 ppb observed.

HIPPO data for N_2O differ radically from model results. Simulations completely miss the major feature of the global distribution, the tropical/subtropical maxima at altitude (Fig. 5c, d), with greater enhancement north of the ITCZ. This pattern has been observed in all six HIPPO cross sections flown to date, although the magnitude of the enhancement aloft was largest in HIPPO-1 southbound. HYSPLIT [Draxler and Rolf, 2010] trajectories showed that air near the surface originated from the east, whereas the air with enhanced N_2O concentrations, above 2 km, came from the west, suggesting sources in regions of convection in the Western Pacific and/or tropical South Asia or Indonesia. Samples collected on the "CARIBIC" flights of commercial aircraft from Germany to India [Schuck et al., 2010], also showed diffuse maxima of N_2O in the upper troposphere (8.5-12 km) during June – August, peaking in the same general latitude range as in HIPPO flights (15-25N). It appears that much of the excess N_2O seen by HIPPO was generated in the tropics, but it is difficult to distinguish land-based sources from possible production by corona discharge or lightning in convective storms (Martinez and Brandvold, 1996) or by other mechanisms.

Previous studies [Hirsch et al., 2006; Huang et al., 2008] using sparse station data already suggested that unaccounted tropical sources were needed to close the N_2O budget. HIPPO data strongly support that view. Elevated concentrations high in the atmosphere found in HIPPO indicate a notably stronger tropical source than could be inferred from surface data only. Even in the North polar region, HIPPO data often showed maximum concentrations of N_2O aloft (cf. Figs 2, 3, 5), emphasizing the difficulty of using surface measurements for modeling of this important species.

Summary and conclusions

HIPPO provides a unique data set for atmospheric research: simultaneous, fine-grained, global, high frequency measurements of major greenhouse gases, tracers

with a wide range of chemical lifetimes and diverse source processes, O_2/N_2 and Ar/N_2 ratios, black carbon, and aerosols, plus the isotopic composition of CO_2. Concentration data from HIPPO are linked to world standards, and multiple measurements provide checks on data quality. The data from all missions will be publicly available within 12-18 months of collection. HIPPO data have already played a major role in calibrating total column measurements of CO_2, CO, and CH_4 from the Total Carbon Column Observing Network (TCCON) of Fourier transform spectrometers [Wunch et al. 2010].

First impressions already highlight new phenomena: dense pollution high over the Arctic in late fall/early winter, with a notable component of black carbon; the imprint of large N_2O sources in the tropical or subtropical areas of Asia or the Western Pacific; and sources of CH_4 in the Arctic both from fossil fuel extraction and from non-industrial sources. Although not discussed here, we also observed short-lived gases emanating from various marine environments across the Pacific (e.g. methyl nitrate, haloforms) and from major industrial areas.

HIPPO data clearly delineate the atmospheric imprint of summertime sinks for CO_2 and sources for O_2 in the southern hemisphere, providing a new tool to infer the strength of ocean and land fluxes in the carbon cycle. Curtain plots reveal large-scale features invisible to satellites and blurred by models, revealing the internal structure of global CO_2 distributions hitherto observed fuzzily by satellites and sparse remote stations.

The most novel aspect of HIPPO is the imaging of the signatures of global atmospheric transport modes with high clarity. From the South Pacific convergence zone and ITCZ, to the cold dome over the winter pole, HIPPO data show the influence of convection, isentropic transport, and stratosphere-troposphere exchange, with fine resolution at global scale. Remarkably sharp gradients in tracer concentrations are observed at airmass boundaries. Inverted tracer gradients, with maxima aloft, were found to be common in both hemispheres over the Pacific. These features present major challenges to global models and to observation systems using sparse surface stations and satellites. If not represented in global inverse model studies, they can lead to major biases and inconsistencies. HIPPO data can play a crucial role in identifying and resolving these issues.

Acknowledgments

The HIPPO Program was supported by NSF grants ATM-0628575, ATM-0628519, and ATM-0628388 to Harvard University, University of California (San Diego), University Corporation for Atmospheric Research, University of Colorado/CIRES, and by the National Center for Atmospheric Research. The National Center for Atmospheric Research is supported by the National Science Foundation. Participation by NOAA instruments, and weather forecasting, were supported in part by the National Science Foundation though its Atmospheric Chemistry Program to CIRES, the National Oceanic and Atmospheric Administration through its Atmospheric Composition and Climate Program and the Office of Oceanic and Atmospheric Research, and the National Aeronautics and Space Administration through its Upper Atmosphere Research Program and Radiation Sciences Program. The AWAS flasks system was supported by NSF grants NSF ATM0849086 and AGS0959853 to the University of Miami. VCSEL was supported by NSF grant AGS-1036275 to Princeton University. We are grateful to the crew of the GV for their dedication and professional skill in making the flights possible and in taking the GV to places not previously visited by a jet aircraft, and to the NCAR Earth Observing Laboratory for support of logistics and public outreach. The authors gratefully acknowledge the NOAA Air Resources Laboratory (ARL) for the provision of the HYSPLIT transport and dispersion model.

Citations

Bethan, S., G. Vaughan, C. Gerbig, A. Volz-Thomas, H. Richer, and D. A. Tiddeman, Chemical air mass differences near fronts, J. Geophys. Res., 103, 13,413–13,434.. 1998

Bey I,, D. J. Jacob, R. M. Yantosca, J. A. Logan, B. D. Field, A. M. Fiore, Q. B. Li, H. G. Y. Liu, M. J. Mickley, M. G. Schultz, Global modeling of tropospheric chemistry with assimilated meteorology: Model description and evaluation J. Geophys. Res.-Atm. 106, 23073-23095, 2001

Chahine, M. T., L. Chen, P. Dimotakis, X. Jiang, Q. Li, E. T. Olsen, T. Pagano, J. Randerson, and Y. L. Yung, Satellite remote sounding of mid-tropospheric CO_2, *Geophys. Res. Lett.,* 35, L17807, doi:10.1029/2008GL035022, 2008.

Cooper, O. R., et al., A case study of transpacific warm conveyor belt transport: Influence of merging airstreams on trace gas import to North America, J. Geophys. Res., 109, D23S08, doi:10.1029/2003JD003624, 2004.

Davis, D. D. (1980), PROJECT GAMETAG - AN OVERVIEW, *Journal of Geophysical Research-Oceans and Atmospheres*, *85*(NC12), 7285-7292.

Daube, B. C., K. A. Boering, A. E. Andrews, and S. C. Wofsy (2002), A high-precision fast-response airborne CO2 analyzer for in situ sampling from the surface to the middle stratosphere, *Journal of Atmospheric and Oceanic Technology*, *19*(10), 1532-1543.

Engelen, R.J., S. Serrar, and F. Chevallier, , Four-dimensional data assimilation of atmospheric CO_2 using AIRS observations. *J. Geophys. Res. 114*, D03303, doi:10.1029/2008JD010739, 2009..

Fujiwara M., et al., "Cirrus observations in the tropical tropopause layer in the western Pacific", *J. Geophys. Res.-Atmos., 114*, D09304, doi:10.1029/2008JD011040, 2009.

Gurney KR, Law RM, Denning AS, Rayner PJ, Baker D, Bousquet P, Bruhwiler L, Chen YH, Ciais P, Fan S, Fung IY, Gloor M, Heimann M, Higuchi K, John J, Maki T, Maksyutov S, Masarie K, Peylin P, Prather M, Pak BC, Randerson J, Sarmiento J, Taguchi S, Takahashi T, Yuen CW, Towards robust regional estimates of CO2 sources and sinks using atmospheric transport models, *Nature 415*, 6872, 626-630, 2002.

Gregory, G. L., et al., "Chemical characteristics of the Pacific tropospheric air in the region of the Intertropical Convergence Zone and South Pacific Convergence Zone", *J. Geophys. Res., 104*, 5677-5696, 1999.

Heimann, M., and S. Körner, 2003: The global atmospheric tracer model TM3. Technical Report No. 5, Max-Planck-Institut für Biogeochemie, Jena, pp. 131.

Hirsch, A. I., A. M. Michalak, L. M. Bruhwiler, W. Peters, E. J. Dlugokencky, and P. P. Tans (2006), Inverse modeling estimates of the global nitrous oxide surface flux from 1998-2001, *Global Biogeochemical Cycles*, *20*(1).

Hoell, J.M., D.D. Davis, D.J. Jacob, M.O. Rodgers, R.E. Newell, H.E. Fuelberg, R.J. McNeal, J.L. Raper, and R.J. Bendura, The Pacific Exploratory Mission in the tropical Pacific: PEM-Tropics A, August-September 1996, *J. Geophys. Res., 104*, 5567-5584, 1999.

Hollingsworth, A., R.J. Engelen, C. Textor, A. Benedetti, O. Boucher, F. Chevallier, A. Dethof, H. Elbern, H. Eskes, J.Flemming, C. Granier, J.W. Kaiser, J. J. Morcrette, P. Rayner, V-.H Peuch, L. Rouil, M. Schultz, A. Simmons, and the GEMS consortium, Toward a monitoring and forecasting system for atmospheric composition. The GEMS Project. *Bull. Amer. Meteor. Soc., 89*, 1147 - 1164, doi:10.1175/2008BAMS2355.1., 2009.

Huang, J., A. Golombek, R. Prinn, R. Weiss, P. Fraser, P. Simmonds, E. J. Dlugokencky, B. Hall, J. Elkins, P. Steele, R. Langenfelds, P. Krummel, G. Dutton, and L. Porter, Estimation of regional emissions of nitrous oxide from 1997 to 2005 using multinetwork measurements, a chemical transport model, and an inverse method *J. Geophys. Res., 113*, D17313, doi:10.1029/2007JD009381, 2008

Ishijima, K., Patra, P. K., Takigawa, M, Machida, T., Matsueda, H, Sawa, Y. , Steele, L. P., Krummel, P. B., Langenfelds, R. L., Aoki, S., and Nakazawa, T., The stratospheric influence on the seasonal cycle of nitrous oxide in the troposphere, deduced from aircraft observations and model simulations, (*J. Geophys. Res., in press, 2010*).

Jacob, D.J., J.H. Crawford, M.M. Kleb, V.S. Connors, R.J. Bendura, J.L. Raper, G.W. Sachse, J.C. Gille, L. Emmons, and C.L. Heald, The Transport and Chemical Evolution over the Pacific (TRACE-P) aircraft mission: design, execution, and first results, *J. Geophys. Res., 108*, 9000, 10.1029/2002JD003276, 2003.

Kort, E. A., J. Eluszkiewicz, B. B. Stephens, J. B. Miller, C. Gerbig, T. Nehrkorn, B. C. Daube, J. O. Kaplan, S. Houweling, and S. C. Wofsy (2008), Emissions of CH4 and N2O over the United States and Canada based on a receptor-oriented modeling framework and COBRA-NA atmospheric observations, *Geophysical Research Letters*, *35*(18).

Machida, T., H. Matsueda, Y. Sawa, Y. Nakagawa, K. Hirotani, N. Kondo, K. Goto, T. Nakazawa, K. Ishikawa, and T. Ogawa (2008), Worldwide Measurements of Atmospheric CO2 and Other Trace Gas Species Using Commercial Airlines, *Journal of Atmospheric and Oceanic Technology*, *25*(10), 1744-1754.

Martinez, P., and D. K. Brandvold, Laboratory and field measurements of NO_x produced from corona discharge, *Atm. Environ. 30*, 4177-4182, 1996.

Nakazawa et al, Temporal and spatial variations of upper tropospheric and lower

stratospheric carbon dioxide, *Tellus B, 43*, 106, DOI: 10.1034/j.1600-0889.1991.t01-1-00005.x, 1991.

Mari, C., et al., "On the relative role of convection, chemistry, and transport over the South Pacific Convergence Zone during PEM-Tropics B: a case study", *J. Geophys. Res.-Atmos., 108*, 8232, doi:10.1029/2001JD001466, 2003.

Marenco, A., et al. (1998), Measurement of ozone and water vapor by Airbus in-service aircraft: The MOZAIC airborne program, An overview, *Journal of Geophysical Research-Atmospheres*, *103*(D19), 25631-25642.

Michalak, A. M., L. Bruhwiler, and P. P. Tans (2004), A geostatistical approach to surface flux estimation of atmospheric trace gases, *Journal of Geophysical Research-Atmospheres*, *109*(D14).

R. Nassar, D.B.A. Jones, P. Suntharalingam, J.M. Chen, R.J. Andres, K.J. Wecht, R.M. Yantosca, S.S. Kulawik, K.W. Bowman, J.R. Worden, T. Machida and H. Matsueda, Modeling global atmospheric CO_2 with improved emission inventories and CO_2 production from the oxidation of other carbon species, *Geoscientific Model Development Discussions, 3*, 889-948, 2010.

Pan, L. L., K. P. Bowman, E. L. Atlas, S. C. Wofsy, F. Zhang, J. F. Bresch, B. A. Ridley, J. V. Pittman, C. R. Homeyer, P. Romashkin, and W. A. Cooper, The Stratosphere-Troposphere Analyses of Regional Transport 2008 Experiment, *Bulletin of the American Meteorological Society, 91*, 3, 327-342, 2010.

Patra, P. K., M. Takigawa, G. S. Dutton, K. Uhse, K. Ishijima, B. R. Lintner, K. Miyazaki, and J. W. Elkins, Transport mechanisms for synoptic, seasonal and interannual SF_6 variations and "age" of air in troposphere, *Atmos. Chem. Phys., 9*, 1209-1225, 2009.

Prasad, S. S., and E. C. Zipf, Atmospheric production of nitrous oxide from excited ozone and its potentially important implications for global change studies, *J. Geophys. Res. 113,* D15307, doi:10.1029/2007JD009447, 2008

Raper, J.L., M.M. Kleb, D.J. Jacob, D.D. Davis, R.E. Newell, H.E. Fuelberg, R.J. Bendura, J.M. Hoell, and R.J. McNeal, Pacific Exploratory Mission in the tropical Pacific: PEM-Tropics B, March-April 1999, *J. Geophys. Res., 106*, 32,401-32,425, 2001

Rastigejev, Y., R. Park, M.P. Brenner, and D.J. Jacob, Resolving intercontinental pollution plumes in global models of atmospheric transport , *J. Geophys. Res., 115,* D02302, 2010

Schwarz, J. P., J. R. Spackman, D. W. Fahey, R. S. Gao, U. Lohmann, P. Stier, L. A. Watts, D. S. Thomson, D. A. Lack, L. Pfister, M. J. Mahoney, D. Baumgardner, J. C. Wilson, J. M. Reeves, Coatings and their enhancement of black-carbon light absorption in the tropical atmosphere, *J. Geophys. Res*., doi:10.1029/2007JD009042, 2008.

Schuck, T. J., C. A. M. Brenninkmeijer, A. K. Baker, F. Slemr, P. F. J. von Velthoven, and A. Zahn Greenhouse gas relationships in the Indian summer monsoon plume measured by the CARIBIC passenger aircraft, Atm. Chem. Phys. 10, 3965-3984, 2010.

Stephens BB, Keeling RF, Paplawsky WJ, Shipboard measurements of atmospheric oxygen using a vacuum-ultraviolet absorption technique, Tellus Series B-Chemical and Physical Meteorology 55, 857-878, 2003

Stephens, B. B., et al. (2007), Weak northern and strong tropical land carbon uptake from vertical profiles of atmospheric CO2, *Science*, *316*(5832), 1732-1735.

Widlansky, M., Variability of the South Pacific Convergence Zone and its influence on the general atmospheric circulation, Masters Thesis, Georgia Institute of Technology, 2007, 76pp.

Wunch, D. *et al.* Calibration of the total carbon column observing network using aircraft profile data, *Atmos. Meas. Tech. Discuss., 3*, 2603-2632, 2010.

M.A. Zondlo, M.E. Paige, S.M. Massick, and J.A. Silver, "Development, flight performance, and calibrations of the NSF Gulfstream-V vertical cavity surface emitting laser (VCSEL) hygrometer", J. Geophys. Res.-Atmospheres, doi:10.1029/2010JD014445, in press, 2010.

Table 1. Measurements and species on the GV in HIPPO. Red symbols denote species with 3 or more measurements, sampling rates in ().

Harvard/Aerodyne—HAIS QCLS	CO_2, CH_4, CO, N_2O (1 Hz)
NCAR AO2	O_2/N_2, CO_2 (0.5 Hz)
Harvard OMS CO_2	CO_2 (0.5 Hz)
NOAA CSD O_3	O_3 (1 Hz)
NOAA GMD O_3, H_2O	O_3, H_2O (1 Hz)
NCAR RAF CO	CO (1 Hz)
NOAA UCATS and PANTHER GCs	CO, CH_4, N_2O, CFCs. HCFCs, SF_6, CH_3Br, PAN, CH_3Cl, H_2, H_2O (1 sample per 70 – 200 s)
Whole Air Sampling: NWAS (NOAA), AWAS (Miami), MEDUSA (NCAR/Scripps)	O_2/N_2, N_2/Ar, CO_2, CH_4, CO, N_2O, other GHGs, halocarbons, SF_6, H_2, COS, CS_2, solvent gases, reactive hydrocarbons, marine species, isotopes of CO_2, …
VCSEL Princeton/SWS	H_2O (1 Hz)
NOAA SP2	Black Carbon mass, size (1 Hz)
MTP, wing stores	T, P, vertical structure, winds, aerosols, cloud water

Figure Captions

Figure 1. (Panels a, b) Locations of flight tracks and vertical profiles (red points) for HIPPO deployments 1 and 2. (Panel c) Vertical profiles in the HIPPO-1 cross section of the Pacific Southbound near the Dateline (Flights 2-7), tropopause heights (pressure altitude, km; cyan) from MTP, and stratospheric flight segments in red. (Panel d) Cross-section of potential temperature (θ) in HIPPO-1, on the southbound leg near the dateline. The white dotted lines mark the flight path of the GV and grey lines show contours of potential temperature. Altitudes are given in meters above sea level (GPS).

Figure 2. Cross-sections of CH_4 (ppb), CO (ppb), CO_2 (ppm), SF_6 (ppt), N_2O (ppb) and H_2O (log_{10} (ppm)) on HIPPO-1, southbound along the dateline, January, 2009. White dashed lines show flight tracks, and grey contours show potential temperature. SF_6 data represent a composite of PANTHER and UCATS data, and H_2O data are from VCSEL. Altitudes are given in meters above seal level (GPS).

Figure 3. (Panels a, b) Cross-sections of CO_2 (ppm) and CO (ppb), on HIPPO-2, southbound along the dateline, November, 2009. Grey contours show potential temperature. (Panel c) Photo of dense layer of dark aerosols, looking north at 80°N, 8 km altitude, 2 Nov. 2009. (Photo: E. Kort); (Panels D, E) Vertical profiles of Black Carbon ("BC") and CO, and CO_2, CH_4 and N_2O at 77.2 N, on HIPPO-2, 2 Nov. 2009.

Figure 4. (Panel a) Meridional gradients of CO_2 averaged between 0.3 and 1.5 km (Δ) and 3.5 – 6.5 km (o). (Panel b) Variation of the O_2:N_2 ratio, as in (a). (Panel c) CO_2 as in (a), from the GEOS-CHEM simulation. Areas of apparent CO_2 uptake and emission are denoted by green and red symbols respectively in Panel c.

Figure 5. Model simulations for HIPPO-1, southbound along the dateline, January, 2009. (Panels a, b) Cross sections of CO_2 (ppm) and SF_6 (ppt) from the GEOS-CHEM and ACTM models, respectively. (Panel c) Vertical profiles of N_2O in the subtropics (ACTM and observed in HIPPO-1), and (d) cross section for N_2O from the ACTM for the HIPPO-1 flight track (Flights 2 – 7).

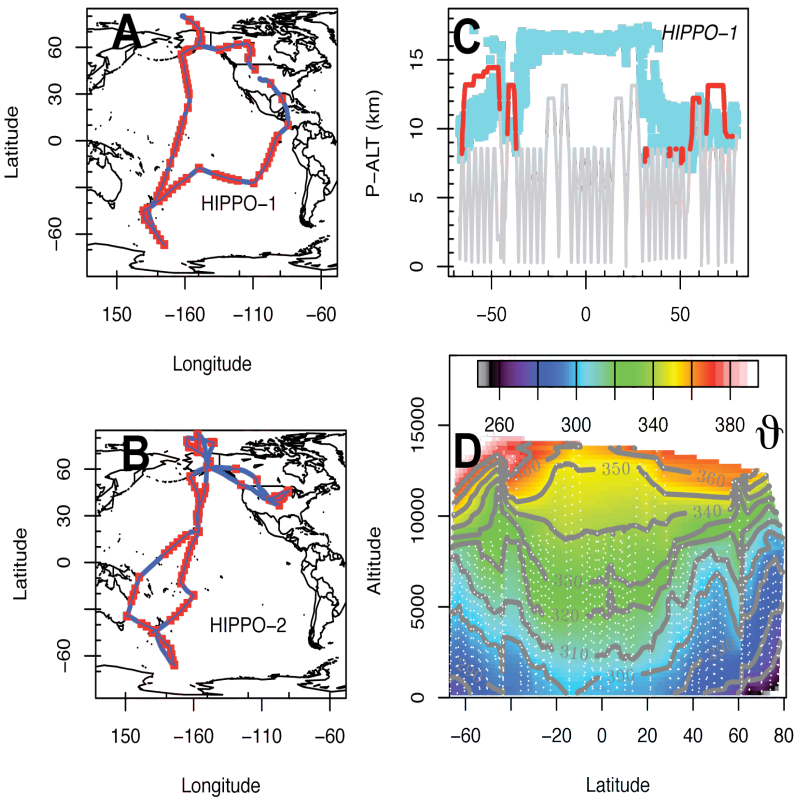

Figure 1. (Panels a, b) Locations of flight tracks and vertical profiles (red points) for HIPPO deployments 1 and 2. (Panel c) Vertical profiles in HIPPO-1 cross section of the Pacific (Flights 2-7), tropopause heights (pressure atltitude, km; cyan) from MTP, and stratospheric flight segments in red. (Panel d) Cross section of potential temperature (ϑ) in HIPPO-1, on the southbound leg near the dateline. The white dotted lines mark the flight path of the GV and grey lines show contours of potential temperature. Altitudes are given in meters above sea level (GPS).

x

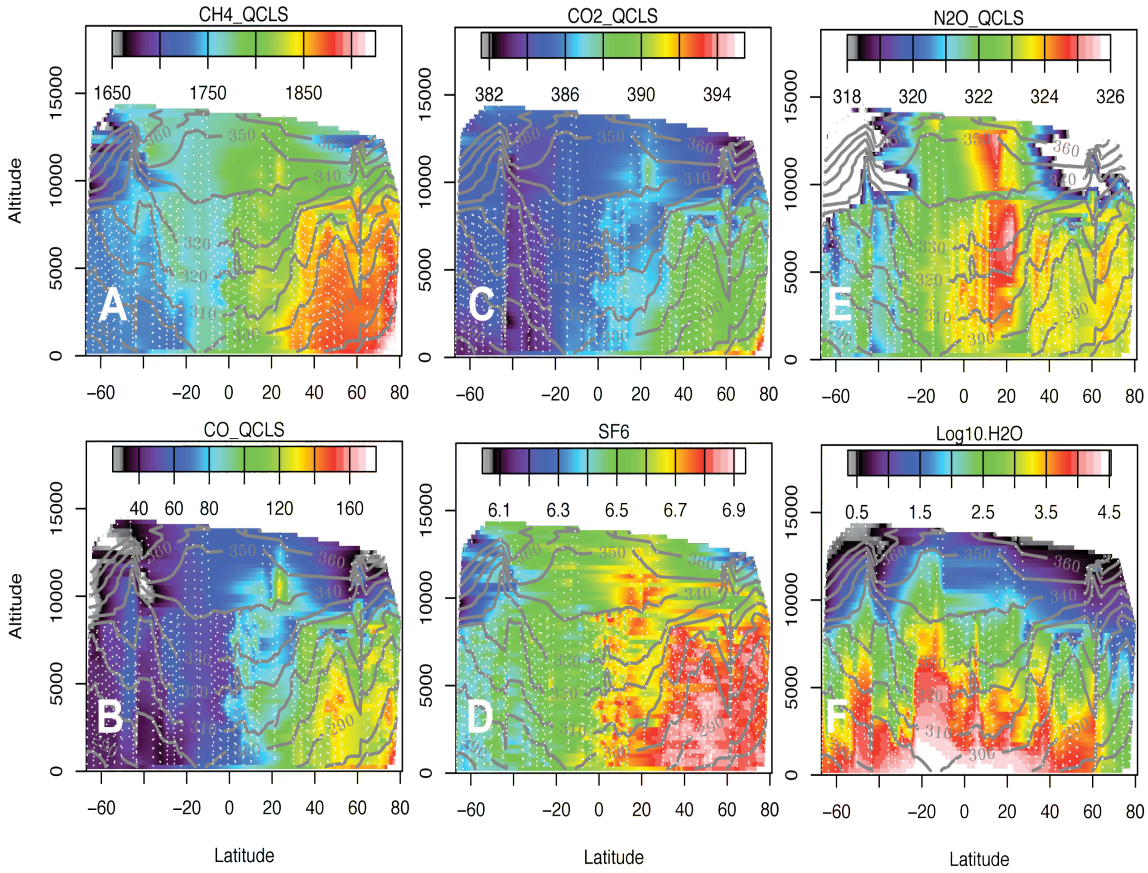

Figure 2. Cross sections of CH_4 (ppb), CO (ppb), CO_2 (ppm), SF_6 (ppt), N_2O (ppb) and H_2O (log_{10} (ppm)) on HIPPO-1, southbound along the dateline, January, 2009. White dashed lines show flight tracks, and grey contours show potential temperature. SF_6 data represent a composite of PANTHER and UCATS data, and H_2O data are from VCSEL.

x

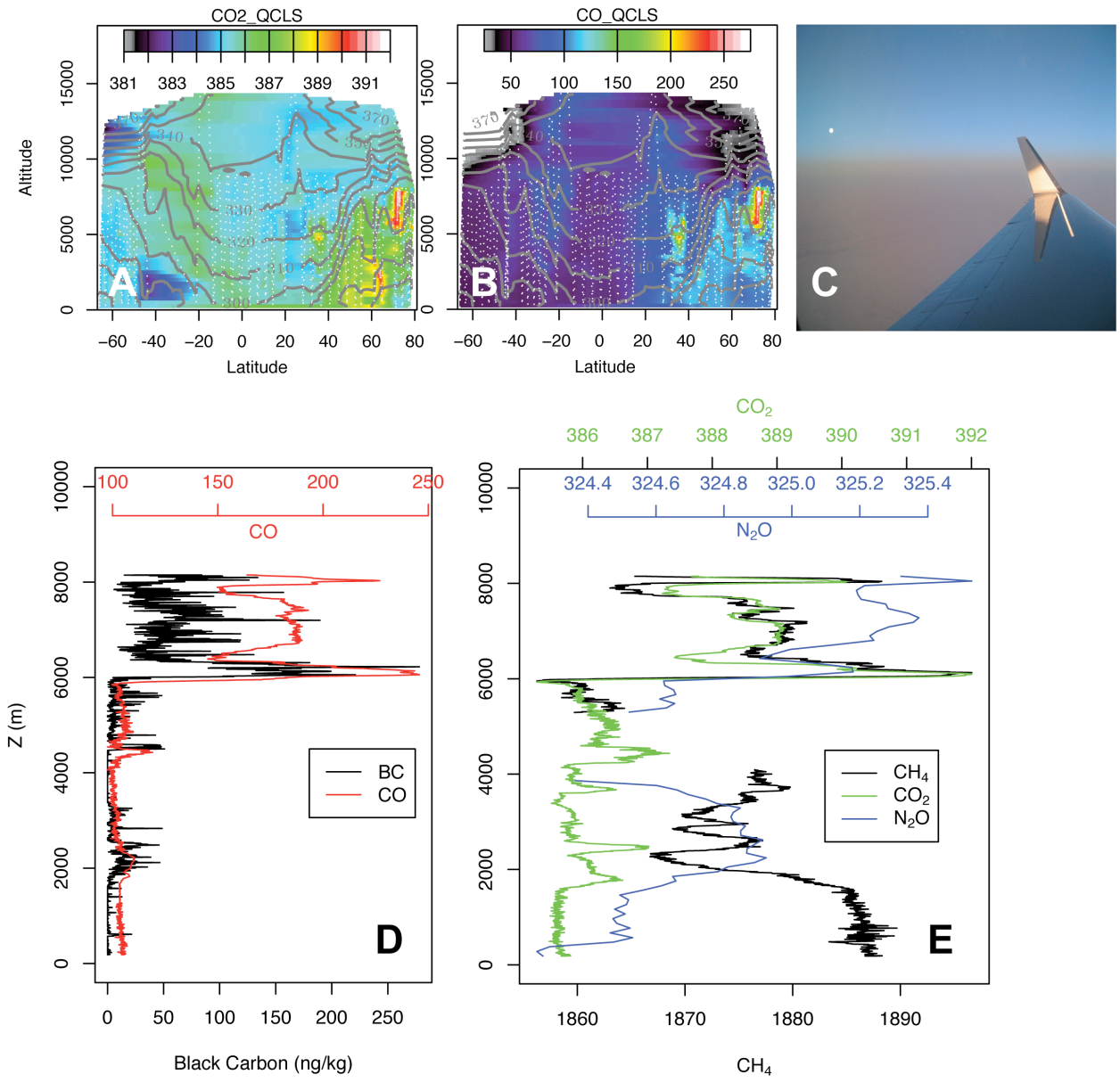

Figure 3. (Panels a, b) Cross sections of CO_2 (ppm) and CO (ppb), on HIPPO-2, southbound along the dateline, November, 2009. Grey contours show potential temperature. (Panel c) Photo of dense layer of dark aerosols, looking north at 80^{o}N, 8 km altitude, 2 Nov. 2009 (Photo: E. Kort); (Panels D, E) Vertical profiles of Black Carbon ("BC") and CO, and CO_2, CH_4 and N_2O at 77.2 N, on HIPPO-2, 2 Nov. 2009.

x

x

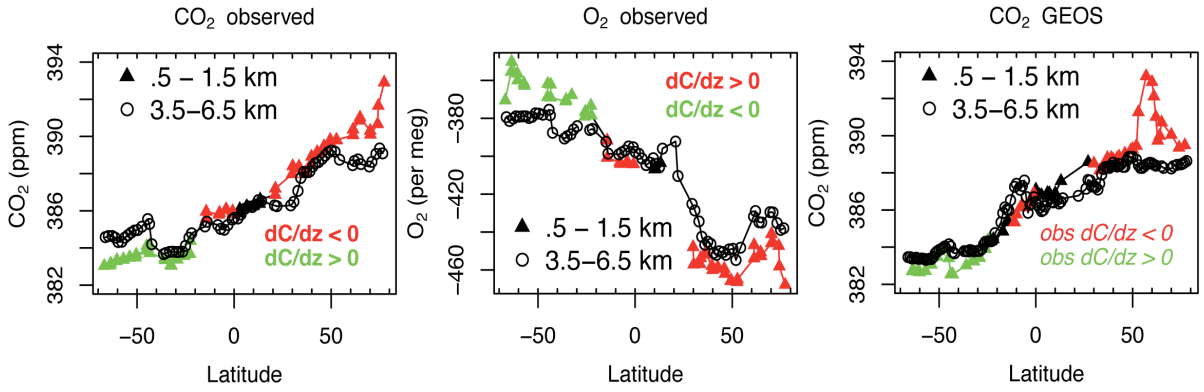

Figure 4. (Panel a) Meridional gradients of CO_2 averaged between 0.5 and 1.5 km (Δ) and 3.5 – 6.5 km (o). (Panel b) Variation of the O_2:N_2 ratio, as in (a). (Panel c) CO_2 as in (a), from the GEOS-CHEM simulation. Areas of apparent CO_2 uptake and emission are denoted by green and red symbols respectively, conversely for O_2.

x

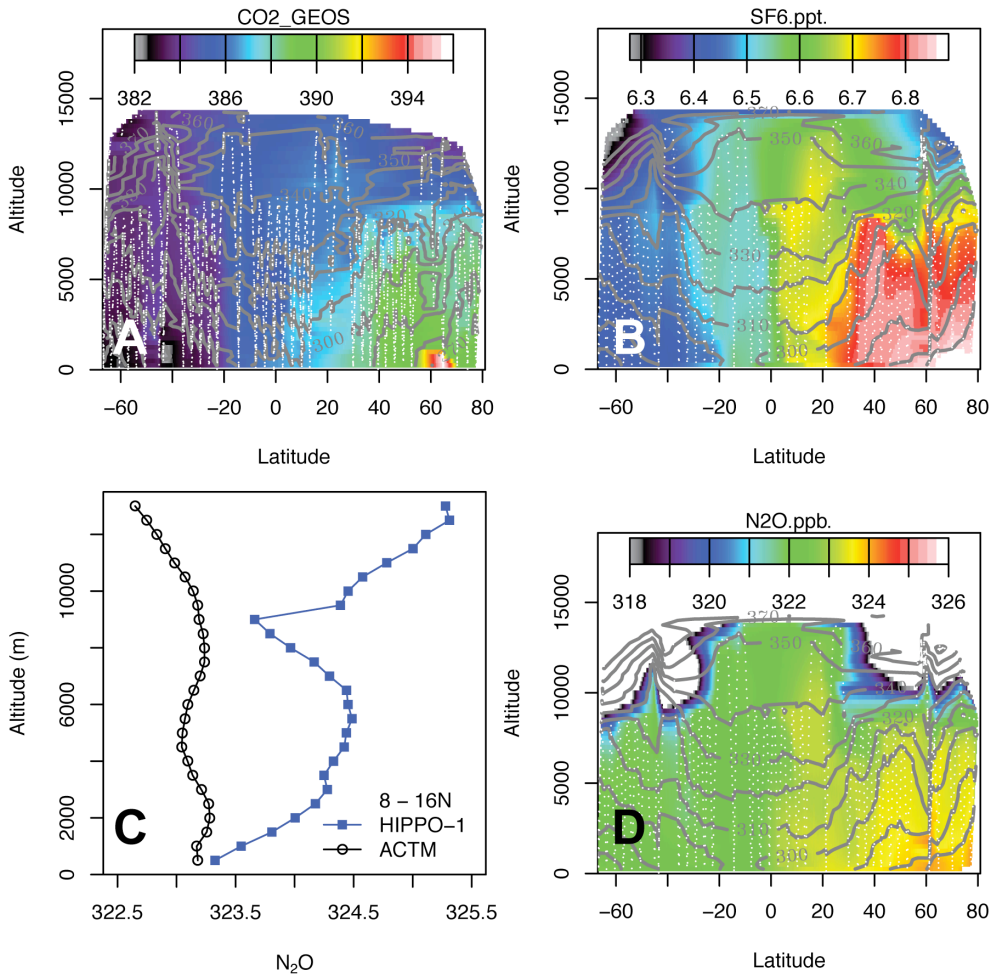

Figure 5. Model simulations for HIPPO-1, southbound along the dateline, January, 2009. (Panels a, b) Cross sections of CO_2 (ppm) and SF_6 (ppt) from the GEOS-CHEM and ACTM models, respectively. (Panel c) Vertical profiles of N_2O in the subtropics (ACTM and observed in HIPPO-1), and (d) cross section for N_2O from the ACTM for the HIPPO-1 flight track.